

Lithium abundance and rotation of seismic solar analogues

Solar and stellar connection from *Kepler* and HERMES observations^{*}

P. G. Beck¹, J.-D. do Nascimento Jr.^{2,3}, T. Duarte², D. Salabert¹, A. Tkachenko⁴, S. Mathis¹,
S. Mathur⁵, R. A. García¹, M. Castro², P. L. Pallé^{6,7}, R. Egeland^{8,9}, D. Montes⁷, O. Creevey¹¹,
M. F. Andersen¹², D. Kamath⁴, and H. van Winckel⁴

- ¹ Laboratoire AIM, CEA/DRF - CNRS - Univ. Paris Diderot - IRFU/SaP, Centre de Saclay, 91191 Gif-sur-Yvette Cedex, France
e-mail: paul.beck@cea.fr
² Departamento de Física, Universidade Federal do Rio Grande do Norte, 59072-970 Natal, RN, Brazil
³ Harvard-Smithsonian Center for Astrophysics, 60 Garden Street, Cambridge, MA 02138, USA
⁴ Instituut voor Sterrenkunde, KU Leuven, B-3001 Leuven, Belgium
⁵ Space Science Institute, 4750 Walnut street Suite 205, Boulder, CO 80301, USA
⁶ Instituto de Astrofísica de Canarias, E-38200 La Laguna, Tenerife, Spain
⁷ Departamento de Astrofísica, Universidad de La Laguna, E-38206 La Laguna, Tenerife, Spain
⁸ High Altitude Observatory, National Center for Atmospheric Research, P.O. Box 3000, Boulder, CO 80307-3000, USA
⁹ Department of Physics, Montana State University, Bozeman, MT 59717-3840, USA
¹⁰ Dpto. Astrofísica, Facultad de CC. Físicas, Universidad Complutense de Madrid, E-28040 Madrid, Spain
¹¹ Laboratoire Lagrange, Université de Nice Sophia-Antipolis, UMR 7293, CNRS, Observatoire de la Côte d'Azur, Nice, France
¹² Stellar Astrophysics Centre, Aarhus University, Ny Munkegade 120, 8000 Aarhus C, Denmark

Received: 30 September 2016 / Accepted: 2 February 2017

ABSTRACT

Context. Lithium abundance $A(\text{Li})$ and surface rotation are good diagnostic tools to probe the internal mixing and angular momentum transfer in stars.

Aims. We explore the relation between surface rotation, $A(\text{Li})$ and age in a sample of seismic solar-analogue stars and we study their possible binary nature.

Methods. We select a sample of 18 solar-analogue stars observed by the NASA *Kepler* satellite for an in-depth analysis. Their seismic properties and surface rotation rates are well constrained from previous studies. About 53 hours of high-resolution spectroscopy were obtained to derive fundamental parameters from spectroscopy and $A(\text{Li})$. These values were combined and confronted with seismic masses, radii and ages, as well as surface rotation periods measured from *Kepler* photometry.

Results. Based on radial velocities, we identify and confirm a total of 6 binary star systems. For each star, a signal-to-noise ratio of $80 \leq S/N \leq 210$ was typically achieved in the final spectrum around the lithium line. We report fundamental parameters and $A(\text{Li})$. By using the surface rotation period derived from *Kepler* photometry, a well-defined relation between $A(\text{Li})$ and rotation was obtained. The seismic radius translates the surface rotation period into surface velocity. With models constrained by the characterisation of the individual mode frequencies for single stars, we identify a sequence of three solar analogues with similar mass ($\sim 1.1 M_{\odot}$) and stellar ages ranging between 1 to 9 Gyr. Within the realistic estimate of $\sim 7\%$ for the mass uncertainty, we find a good agreement between the measured $A(\text{Li})$ and the predicted $A(\text{Li})$ evolution from a grid of models calculated with the Toulouse-Geneva stellar evolution code, which includes rotational internal mixing, calibrated to reproduce solar chemical properties. We found a scatter in ages inferred from the global seismic parameters, too large when compared with $A(\text{Li})$.

Conclusions. We present Li-abundance for a consistent spectroscopic survey of solar-analogue stars with a mass of $1.00 \pm 0.15 M_{\odot}$, and characterised through asteroseismology and surface rotation rates based on *Kepler* observations. The correlation between $A(\text{Li})$ and P_{rot} supports the gyrochronological concept for stars younger than the Sun and becomes clearer, if the confirmed binaries are excluded. The consensus between measured $A(\text{Li})$ for solar analogues with model grids, calibrated onto the Sun's chemical properties suggests that these targets share the same internal physics. In this light, the solar Li and rotation rate appear to be normal for a star like the Sun.

Key words. stars: fundamental parameters – stars: solar-type – stars: rotation – stars: evolution – Methods: observational

1. Introduction

In the last decade, numerous studies focused on the question whether the rotation and chemical abundances of the

Sun are typical for a solar-type star, i.e. a star of a solar mass and age (e.g. Gustafsson 1998; Allende Prieto et al. 2006; Delgado Mena et al. 2014; Datzon et al. 2014; Ramírez et al. 2014; Carlos et al. 2016; dos Santos et al. 2016). These studies compared the Sun with solar-like stars and were inconclusive due to relatively large systematic errors (Gustafsson 2008; Robles et al. 2008; Reddy et al. 2003).

^{*} Based on observations made with the NASA *Kepler* space telescope and the HERMES spectrograph mounted on the 1.2 m MERCATOR Telescope at the Spanish Observatorio del Roque de los Muchachos of the Instituto de Astrofísica de Canarias.

Table 1. Parameters found in the literature of the stars used in this study.

| KIC | ν_{\max} [μHz] | M [M_{\odot}] | R [R_{\odot}] | P_{rot} [days] | Age [Gyr] | Ref. |
|-----------|------------------------------------|----------------------|----------------------|----------------------------|----------------|------|
| 3241581* | 2969 \pm 17 | 1.04 \pm 0.02 | 1.08 \pm 0.10 | 26.3 \pm 2.0 | 3.8 \pm 0.6 | 1 |
| 3656476* | 1947 \pm 78 | 1.10 \pm 0.03 | 1.32 \pm 0.01 | 31.7 \pm 3.5 | 8.9 \pm 0.4 | 2 |
| 4914923* | 1844 \pm 73 | 1.04 \pm 0.03 | 1.34 \pm 0.02 | 20.5 \pm 2.8 | 7.0 \pm 0.5 | 2 |
| 5084157 | 1788 \pm 14 | 1.06 \pm 0.13 | 1.36 \pm 0.08 | 22.2 \pm 2.8 | 7.8 \pm 3.4 | 3 |
| 5774694 | 3671 \pm 20 | 1.06 \pm 0.05 | 1.00 \pm 0.03 | 12.1 \pm 1.0 | 1.9 \pm 1.8 | 3 |
| 6116048* | 2098 \pm 84 | 1.05 \pm 0.03 | 1.23 \pm 0.01 | 17.3 \pm 2.0 | 6.1 \pm 0.5 | 2 |
| 6593461 | 2001 \pm 18 | 0.94 \pm 0.16 | 1.29 \pm 0.07 | 25.7 \pm 3.0 | 10.7 \pm 4.4 | 3 |
| 7296438* | 1846 \pm 73 | 1.10 \pm 0.02 | 1.37 \pm 0.01 | 25.2 \pm 2.8 | 6.4 \pm 0.6 | 2 |
| 7680114* | 1709 \pm 58 | 1.09 \pm 0.03 | 1.40 \pm 0.01 | 26.3 \pm 1.9 | 6.9 \pm 0.5 | 2 |
| 7700968 | 2010 \pm 25 | 1.00 \pm 0.12 | 1.21 \pm 0.06 | 36.2 \pm 4.2 | 7.5 \pm 3.1 | 3 |
| 9049593 | 1983 \pm 13 | 1.13 \pm 0.14 | 1.40 \pm 0.06 | 12.4 \pm 2.5 | 6.4 \pm 3.4 | 3 |
| 9098294* | 2347 \pm 84 | 0.98 \pm 0.02 | 1.15 \pm 0.01 | 19.8 \pm 1.3 | 8.2 \pm 0.5 | 2 |
| 10130724 | 2555 \pm 27 | 0.85 \pm 0.12 | 1.08 \pm 0.05 | 32.6 \pm 3.0 | 13.8 \pm 5.0 | 3 |
| 10215584 | 2172 \pm 28 | 0.99 \pm 0.13 | 1.12 \pm 0.05 | 22.2 \pm 2.9 | 6.8 \pm 3.5 | 3 |
| 10644253* | 2892 \pm 157 | 1.09 \pm 0.09 | 1.09 \pm 0.02 | 10.9 \pm 0.9 | 0.9 \pm 0.3 | 2 |
| 10971974 | 2231 \pm 6 | 1.04 \pm 0.12 | 1.09 \pm 0.03 | 26.9 \pm 4.0 | 5.8 \pm 3.0 | 3 |
| 11127479 | 1983 \pm 7 | 1.14 \pm 0.12 | 1.36 \pm 0.06 | 17.6 \pm 1.8 | 5.1 \pm 2.2 | 3 |
| 11971746 | 1967 \pm 23 | 1.11 \pm 0.14 | 1.35 \pm 0.06 | 19.5 \pm 2.1 | 6.0 \pm 2.8 | 3 |

Notes. *Kepler* input catalogue (KIC) number, central frequency of the oscillation power excess ν_{\max} by [Chaplin et al. \(2014\)](#), stellar mass and radius in solar units from seismology, surface rotation period P_{rot} from [García et al. \(2014\)](#), stellar age from seismic modelling and reference to the published seismic studies: [1] [García et al. \(in prep, see also Beck et al. 2016\)](#), [2] [Creevey et al. \(2016\)](#) and [3] [Chaplin et al. \(2014\)](#). Stars, for which the parameters were obtained through the detailed-modelling approach as described in Section 2, are flagged with an asterisk.

The fragile element lithium is a distinguished tracer of mixing processes and loss of angular momentum inside a star ([Talon & Charbonnel 1998](#)). Its abundance in stars changes considerably over the lifetime. For low-mass stars during the main sequence, proton-capture reactions destroy most of the initial stellar Li content in the stellar interior. Only a small fraction of the original Li is preserved in the cool, outer convective envelopes. The solar photospheric Li abundance $A(\text{Li})$ is 1.05 ± 0.10 dex ([Asplund et al. 2009](#)). This value is substantially lower than the protosolar nebular abundance of $A(\text{Li}) = 3.3$ dex ([Asplund et al. 2009](#)) measured from meteorites and illustrates that the lithium surface abundance does not reflect the star’s original abundance. A comparison between the Sun and typical stars of one solar mass and solar metallicity in the thin galactic disc by [Lambert & Reddy \(2004\)](#) showed the Sun as “lithium-poor” by a factor of 10. Because the temperature at the base of the solar convective zone is not hot enough to destroy lithium, this large depletion in the observed solar to the meteoritic Li abundance by a factor of 160 remains as one of the biggest challenges of standard solar models. This is known as the solar Li problem (e.g. [Maeder 2009](#); [Meléndez et al. 2010](#), and references therein).

There are two major challenges for understanding the Li abundance in stars similar to the Sun. First, for stars with masses $M \leq 1.1 M_{\odot}$, there is a strong dependence of $A(\text{Li})$ on mass and metallicity, which are governed by the depth of the convective envelope for these stars ([do Nascimento et al. 2009](#); [do Nascimento, Jr. et al. 2010](#); [Baumann et al. 2010](#); [Castro et al. 2016](#)). While the stellar chemical composition can be determined from optical spectroscopy, the mass of a star is a difficult task when a star does not belong to a cluster. In this context, solar analogues, following the classical definition of [Cayrel de Strobel \(1996\)](#), constitute a homogeneous set of stars in which mass and metallicity are well constrained with values close to solar ones as defined before. Fortunately, asteroseismology is a tool that provides precise and accurate values for mass, radius as well as ages of oscillating stars

(e.g. [Aerts, Christensen-Dalsgaard, & Kurtz 2010](#)). The highest level of accuracy of the parameters determined through seismology is reached when the models are constrained by individual frequencies and combined with results from high-resolution spectroscopy (e.g. [Chaplin et al. 2011, 2014](#); [Lebreton & Goupil 2014](#)).

The second unknown is the complex interplay of various transport mechanisms and their efficiency inside the stellar interior and with stellar rotation. Standard models, that only include mixing through convective motion, fail to model the general trend of the $A(\text{Li})$ evolution. This indicates that additional mixing processes have to be taken into account, such as microscopic diffusion ([Eddington 1916](#); [Chapman 1917](#)), inertial gravity waves ([GarcíaLopez & Spruit 1991](#); [Schatzman 1996](#); [Charbonnel & Talon 2005](#)) and the effects of stellar rotation. Rotation has a substantial impact on the stellar evolution (e.g. [Zahn 1992](#); [Maeder & Zahn 1998](#); [Brun et al. 1999](#); [Mathis et al. 2004](#); [Maeder 2009](#); [Ekström et al. 2012](#), and references therein) and can change the properties of solar-type stars by reducing the effects of atomic diffusion, and inducing extra mixing. More specifically, observations of light element abundances bring precise constraints for mixing in models and transport processes in stars ([Talon & Charbonnel 1998](#); [Charbonnel & do Nascimento 1998](#); [Pinsonneault 2010](#); [Somers & Pinsonneault 2016](#)).

Numerous observational and theoretical studies have explored the Li surface abundance in the context of rotation, stellar evolution, age and angular momentum transport (e.g. [van den Heuvel & Conti 1971](#); [Skumanich 1972](#); [Rebolo & Beckman 1988](#); [Zahn 1992, 1994](#); [Charbonnel et al. 1994](#); [Talon & Charbonnel 1998](#); [Charbonnel & do Nascimento 1998](#); [King et al. 2000](#); [Clarke et al. 2004](#); [Talon & Charbonnel 2005](#); [Pinsonneault 2010](#); [Bouvier et al. 2016](#); [Somers & Pinsonneault 2016](#), and references therein). Recently, [Bouvier et al. \(2016\)](#) showed that a rotation-lithium relation exists already at an age of 5 Myrs and also exhibits a significant dispersion. Moreover, [Bouvier](#)

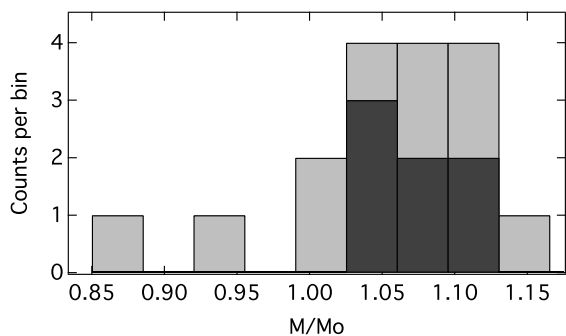


Fig. 1. Distributions of the stellar mass from seismology for the 18 solar-analogue stars in the presented sample. The grey bars flag the total distributions, while the dark shaded areas indicated the distribution of stars with detailed seismic modelling

(2008) proposed a possible link between lithium depletion and the rotational history of exoplanet-host stars. Thus, authors seek a complete and coherent description of the influence of rotation on the lithium abundances on the main-sequence of solar-type stars. A particular challenge for studying $A(\text{Li})$ as a function of the stellar rotation is the surface rotation velocity. If determined from spectroscopy through the Doppler broadening of the absorption lines, only the projected surface velocity $v \sin i$ could be measured, where the axis of the rotation axis remains unknown. If the surface rotation rate is determined through modulation of photometry or activity proxies, one measures the angular velocity in terms of surface rotation period, because a precise measure of the stellar radius is missing.

Understanding the evolution of the lithium abundance as a function of the mass, metallicity and rotation and explaining its dispersion in G dwarfs, is critical to construct a comprehensive model of the Sun as a star (e.g. Pace et al. 2012; Castro et al. 2016). Comparing the measured value of $A(\text{Li})$ in solar analogues with predictions from evolutionary models, calibrated onto the solar case will allow to test the evolution of the Li dilution for typical ‘Suns’ at different ages. This gives us the possibility to test if the mixing processes, assumed to act in the Sun, are peculiar or if the solar lithium value is normal.

This paper is structured as follows: In Section 2, we set the stars to be studied. Its properties and the new spectroscopic parameters are described. From the observations, the relation between lithium and rotation is discussed in Section 3. In Section 4, the measured $A(\text{Li})$ is confronted with theoretical predictions from the Toulouse-Geneva stellar evolution code (TGEC, Hui-Bon-Hoa 2008; do Nascimento et al. 2009) and we compare age estimates from seismology derived from previous studies using different approaches. Conclusions of this work are summarised in Section 5.

2. Data set and stellar parameters

The sample of solar analogues investigated in this study is composed by the 18 stars presented in Salabert et al. (2016a). A summary of the main global properties of these stars are shown in Table 1. The stellar masses, radii and ages reported in the literature (Table 1) were obtained by either grid-modelling analysis of the global-seismic parameters or by using individual frequencies and high-resolution spectroscopy (hereafter also referred to as *detailed* modelling). For a specific discussion of the different modelling approaches, we refer the reader to Lebreton & Goupil (2014). Detailed modelling using individual frequencies with

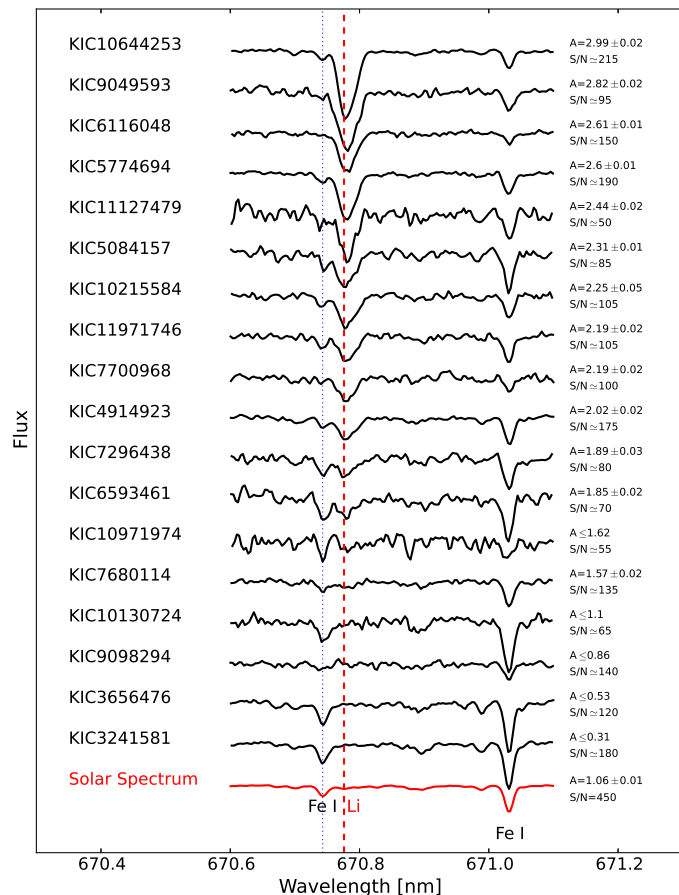


Fig. 2. Lithium doublet observed in the full dataset, sorted from strong to weak lithium lines (top to bottom, respectively). The solar spectrum (red) is shown in the bottom of the diagram. The centre of the lithium and the neighbouring iron line are flagged through the vertical dashed line and blue dotted line, respectively. The achieved S/N, measured lithium abundances as well as upper limits of $A(\text{Li})$ are indicated in the right side.

the *Asteroseismic Modeling Portal* (AMP, Metcalfe et al. 2009) is available for the following stars KIC 3656476, KIC 4914923, KIC 6116048, KIC 7296438, KIC 7680114, KIC 9098294, and KIC 10644253, which were modelled by Mathur et al. (2012), Metcalfe et al. (2014) and Creevey et al. (2016). In this paper we use whenever possible, the latest results of Creevey et al. (2016). An additional star, KIC 3241581, has been modelled by Garcia et al. (in prep., see also Beck et al. 2016), using the *Modules for Experiments in Stellar Astrophysics* (MESA, Paxton et al. 2013, and references therein). For the remaining 10 stars, we adopted the masses and ages obtained by Chaplin et al. (2014) using global seismic parameters determined from 1-month long *Kepler* time series and constraints on temperature and metallicity from multicolour photometry. The mass distribution in Figure 1 shows that this sample mainly consists of stars with masses in the upper half of the allowed mass regime for solar analogues (1–1.15 M_{\odot}). The dark shaded regions in Figure 1 depict the distribution of the stars for which detailed seismic modelling was performed (Mathur et al. 2012; Metcalfe et al. 2014; Creevey et al. 2016, Garcia et al., in prep.). Whenever applicable, we distinguish in the diagrams represented in this paper the values originating from the two analysis approaches.

Surface rotation periods (P_{rot}), measured by García et al. (2014), are reported in Table 1. Selecting oscillating targets with known rotation periods adds a constraint that these stars are mag-

Table 2. Summary of the seismic solar analogue observations.

| KIC | V [mag] | N | ToT [hrs] | ΔT [days] | \overline{RV} [km/s] | ΔRV [km/s] | comment |
|----------|------------|--------|--------------|----------------------|---------------------------|-----------------------|----------------------------|
| 3241581* | 10.35±0.04 | 24 | 9.3 | 709.1 | -30.68 | 0.96 | binary |
| 3656476 | 9.55±0.02 | 6 | 2.5 | 351.1 | -13.23 | 0.14 | |
| 4914923 | 9.50±0.02 | 7 | 2.1 | 297.3 | -31.16 | 2.11 | binary |
| 5084157 | 11.56±0.12 | 10 | 5.2 | 300.1 | -19.66 | 0.21 | |
| 5774694 | 8.37±0.01 | 7 | 1.3 | 348.1 | -17.67 | 0.16 | |
| 6116048 | 8.47±0.01 | 5 | 1.0 | 347.2 | -53.28 | 0.17 | |
| 6593461 | 11.22±0.10 | 9 | 4.1 | 296.2 | -35.39 | [0.37] | large scatter |
| 7296438 | 10.13±0.03 | (+2) 4 | 1.5 | 350.2 | -2.08 | 16.65 | Binary (KOI 364.01) |
| 7680114 | 10.15±0.04 | 8 | 3.4 | 351.0 | -58.96 | 0.180 | |
| 7700968 | 10.37±0.04 | (+2) 4 | 1.4 | 299.1 | +39.47 | 27.62 | binary |
| 9049593 | 10.35±0.04 | 4 | 1.5 | 299.1 | -21.02 | 0.24 | |
| 9098294 | 9.91±0.03 | 7 | 2.6 | 346.1 | -55.78 | 41.35 | binary |
| 10130724 | 12.03±0.19 | 7 | 2.8 | 299.1 | -54.51 | 2.12 | binary |
| 10215584 | 10.62±0.05 | 6 | 2.7 | 337.0 | -11.02 | 0.25 | |
| 10644253 | 9.26±0.02 | 14 | 5.9 | 416.0 | -19.01 | 0.18 | |
| 10971974 | 11.05±0.07 | 4 | 1.6 | 300.1 | -34.58 | 0.27 | |
| 11127479 | 11.21±0.09 | 5 | 2.1 | 300.2 | -29.33 | 0.30 | KOI 2792.01, large scatter |
| 11971746 | 11.00±0.07 | 8 | 3.6 | 301.0 | -44.20 | 0.22 | |

Notes. The star's identifier in the *Kepler* input catalogue (KIC), apparent magnitude in Johnson V, number N of spectra (in bracket the number of additional spectra with S/N only high enough to determine the radial velocity), total accumulated time on target (ToT), the time base ΔT covered by the observations, the mean radial velocity (\overline{RV}), and the difference between the positive and negative extrema of the measured RV values and their internal error, and a comment on the star/system. KOI stand for *Kepler Objects of Interests* and indicates planet host star candidates.

Table 3. Fundamental parameters of the solar analogues from the spectroscopic analysis of HERMES data.

| KIC | T_{eff} [K] | $\log g$ [dex] | v_{min} [km/s] | $v \sin i$ [km/s] | [Fe/H] [dex] | A(Li) [dex] | S/N (Li) |
|----------|-------------------------|-------------------|----------------------------|----------------------|-----------------|----------------|-------------|
| 3241581 | 5685±59 | 4.3±0.1 | 1.0±0.2 | 4.0±0.6 | 0.22±0.04 | ≤0.31 | 180 |
| 3656476 | 5674±50 | 4.2±0.1 | 1.1±0.1 | 4.1±0.7 | 0.25±0.04 | ≤0.51 | 120 |
| 4914923 | 5869±74 | 4.2±0.1 | 1.2±0.1 | 5.0±0.6 | 0.12±0.04 | 2.02±0.02 | 175 |
| 5084157 | 5907±60 | 4.2±0.1 | 1.1±0.1 | 4.8±0.7 | 0.24±0.04 | 2.31±0.01 | 85 |
| 5774694 | 5962±59 | 4.6±0.1 | 1.0±0.2 | 5.5±0.7 | 0.10±0.03 | 2.60±0.01 | 190 |
| 6116048 | 6129±97 | 4.3±0.2 | 1.3±0.2 | 5.8±0.6 | -0.18±0.05 | 2.61±0.01 | 150 |
| 6593461 | 5803±126 | 4.4±0.2 | 1.3±0.3 | 4.8±0.8 | 0.25±0.09 | 1.85±0.02 | 70 |
| 7296438 | 5854±64 | 4.3±0.1 | 1.2±0.2 | 4.5±0.8 | 0.24±0.05 | 1.89±0.03 | 80 |
| 7680114 | 5978±107 | 4.3±0.2 | 1.2±0.3 | 4.4±0.7 | 0.15±0.07 | 1.57±0.02 | 135 |
| 7700968 | 5992±144 | 4.4±0.3 | 1.4±0.4 | 5.3±0.7 | -0.18±0.08 | 2.19±0.02 | 100 |
| 9049593 | 6009±151 | 4.3±0.3 | 1.5±0.3 | 7.2±0.6 | 0.20±0.08 | 2.82±0.02 | 95 |
| 9098294 | 5913±67 | 4.4±0.1 | 1.0±0.2 | 4.7±0.7 | -0.14±0.04 | ≤0.86 | 140 |
| 10130724 | 5649±95 | 4.3±0.2 | 0.9±0.3 | 4.4±0.9 | 0.27±0.09 | ≤1.10 | 65 |
| 10215584 | 5888±67 | 4.3±0.1 | 1.1±0.2 | 5.1±0.6 | 0.05±0.04 | 2.25±0.05 | 105 |
| 10644253 | 6117±64 | 4.4±0.2 | 0.9±0.2 | 4.3±0.6 | 0.11±0.04 | 2.99±0.02 | 215 |
| 10971974 | 5895±114 | 4.4±0.2 | 1.2±0.3 | 4.8±0.8 | 0.02±0.07 | ≤1.62 | 55 |
| 11127479 | 5884±116 | 4.4±0.3 | 1.5±0.3 | 6.1±0.7 | 0.11±0.08 | 2.44±0.02 | 50 |
| 11971746 | 5953±63 | 4.3±0.1 | 1.2±0.2 | 4.5±0.8 | 0.18±0.04 | 2.19±0.02 | 105 |

Notes. The star's identifier in the *Kepler* input catalogue, the effective temperature T_{eff} , the surface acceleration $\log g$, the micro turbulence v_{min} , the projected surface rotational velocity $v \sin i$, the stellar metallicity, and the abundance of lithium are given with their respective uncertainties. Upper limits of the measured A(Li) are indicated for stars with low lithium abundance as consequence of insufficient S/N in the spectra. The last column reports the signal-to-noise ratio around the lithium line.

netically active. However, they are not too active to suppress oscillations. This is another characteristic of our host star.

2.1. Spectroscopic observations

To guarantee a homogenous sample of fundamental parameters, we obtained for each target high-resolution spectra with the HERMES spectrograph (Raskin et al. 2011; Raskin 2011), mounted to the 1.2m MERCATOR telescope, La Palma, Canary Island, Spain.

The observations were performed in four observing runs of 3 to 6 days each. In 2015, spectroscopic data was obtained in June and July, while in 2016 observations were obtained in April and May. The overview on the observations is presented in Table 2. In total 53.1 hrs worth of exposure time were collected. The HERMES spectra cover a wavelength range between 375 and 900 nm with a spectral resolution of $R \approx 85\,000$. The wavelength reference was obtained from emission spectra of Thorium-Argon-Neon reference frames in close proximity to the individual exposure.

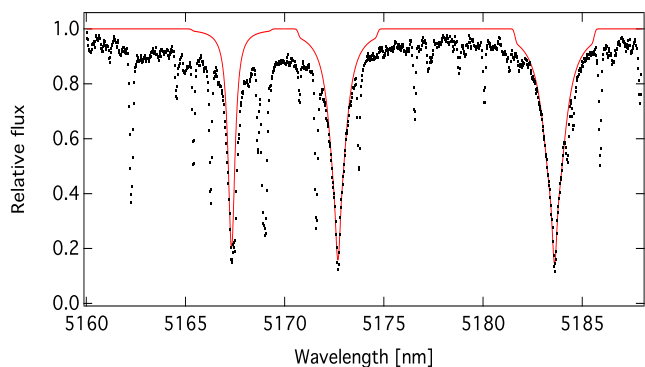


Fig. 3. Mg triplet in the star KIC 7700968. The observed and synthetic spectra are represented by black dots and solid line, respectively.

The spectral reduction was performed with the instrument-specific pipeline (Raskin et al. 2011; Raskin 2011). The radial velocity (RV) for each individual spectrum was determined from the cross correlation of the stellar spectrum in the wavelength range between 478 and 653 nm with a standardised G2-mask provided by the HERMES pipeline toolbox. For HERMES, the 3σ level of the night-to-night stability for the observing mode described above is ~ 300 m/s, which is used as the classical threshold for RV variations to detect binarity. Using Beck et al. (2016) methods we corrected individual spectra for the Doppler shift before normalisation and the process of combining individual spectra. The signal-to-noise ratios (S/N) of each combined spectrum around 670 nm is reported in Table 3 and in Figure 2. A solar flux spectrum was observed with the same HERMES instrument setup in reflected sunlight from the Jovian moon Europa (Beck et al. 2016). This spectrum has a S/N ~ 450 (Figure 2).

2.2. Fundamental parameters

To determine the fundamental parameters, we started with effective temperature T_{eff} , surface gravity $\log g$, metallicity [Fe/H], and micro turbulence v_{min} and projected surface rotational velocity $v \sin i$ from an analysis with the *Grid Search in Stellar Parameters* (gssp¹) software package (Lehmann et al. 2011; Tkachenko et al. 2012; Tkachenko 2015). The library of synthetic spectra were computed using the SYNTHV radiative transfer code (Tsymbal 1996) based on the LLMODELS code (Shulyak et al. 2004). Then, we used the HERMES high-quality spectra to determine the final stellar fundamental parameters (T_{eff} , $\log g$, [Fe/H]) and lithium abundance. We employed the excitation/ionisation equilibrium balance technique to find the stellar parameters that produced consistent abundances of Fe I and Fe II, and by using the solar reference value as described by Meléndez et al. (2012), and Ramírez et al. (2014). For all stars in the sample we determined the fundamental stellar parameters by performing a differential excitation-ionization equilibrium from the abundances of Fe I and Fe II, and by using the solar value as a reference, as described by Meléndez et al. (2012), Monroe et al. (2013), Meléndez et al. (2014b) and Ramírez et al. (2014). We combined Kurucz atmospheric models (Castelli & Kurucz 2004) with equivalent width (EW) measurements of Fe I and Fe II and the 2014 version of the 1D LTE code MOOG (Snedden 1973). The EW were determined from the automated code ARES

¹ The GSSP package is available for download at <https://fys.kuleuven.be/ster/meetings/binary-2015/gssp-software-package>.

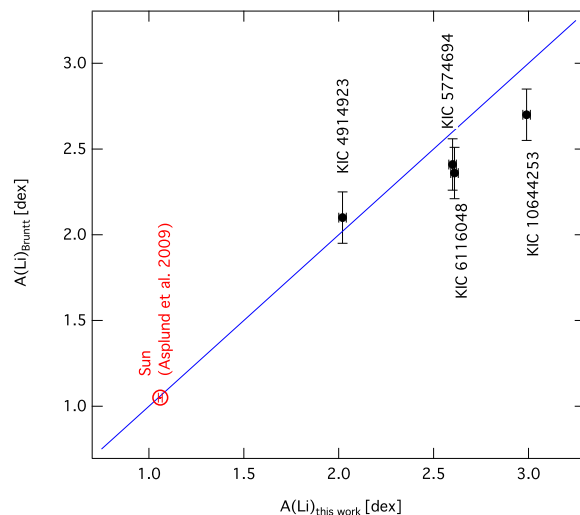


Fig. 4. Comparison of the measured lithium abundances with values from the literature (see Table 4). Black squares flag the four stars from our sample that are overlapping with the Bruntt et al. (2012). The red circle depicts the comparison of the solar lithium abundance derived from our spectrum with the canonical value by Asplund et al. (2009). The blue line denotes the 1:1 ratio between the two datasets.

Table 4. Comparison of lithium abundances with other values in the literature.

| Star | A(Li) [dex] | | Literature reference |
|--------------|-----------------|----------------|----------------------|
| | This work | Literature | |
| KIC 4914923 | 2.02 ± 0.02 | 2.1 ± 0.2 | B12 |
| KIC 5774694 | 2.6 ± 0.01 | 2.4 ± 0.2 | B12 |
| KIC 6116048 | 2.61 ± 0.01 | 2.4 ± 0.2 | B12 |
| KIC 10644253 | 2.99 ± 0.02 | 2.7 ± 0.2 | B12 |
| Sun | 1.06 ± 0.01 | 1.05 ± 0.1 | A09 |

Notes. The stellar identifier, the lithium abundance derived in this work as well as in the literature value, provided by Bruntt et al. (2012) (B12) or Asplund et al. (2009) (A09). The comparison is depicted in Figure 4.

(Sousa et al. 2007). We applied the same method for all stars in our sample, considering the same regions of continuum. Final spectroscopic parameters for the stars are given in Table 3. Formal uncertainties of the stellar parameters were computed as in Epstein et al. (2010) and Bensby et al. (2014). The median metallicity for the sample is 0.15 dex. We note that we find a higher temperature for KIC 10644253, compared to the previous findings of Salabert et al. (2016b). We adopt this new value, because the analysis was improved through increased observing time and by applying a differential analysis, with the HERMES solar spectrum. We adopt the values in Table 3. For KIC 3241581, we confirm the results reported previously by Beck et al. (2016).

The wings of Balmer and Mg-lines in cool dwarfs stars are highly sensitive to the temperature, $\log g$ and metallicity (Gehren 1981; Fuhrmann et al. 1993; Barklem & O'Mara 2001). These lines are formed in deep layers of the stellar atmosphere and they are expected to be insensitive to the non-LTE effects (Barklem 2007), although they depend on convection (Ludwig et al. 2009). The comparison between the observed and synthetic spectra for the region between 516.0 and 518.8 nm, containing the Mg-triplet and a sufficient number of metal lines, shown in Figure 3. The agreement of the line widths shows the quality of our determined fundamental parameters (T_{eff} , $\log g$, [Fe/H]).

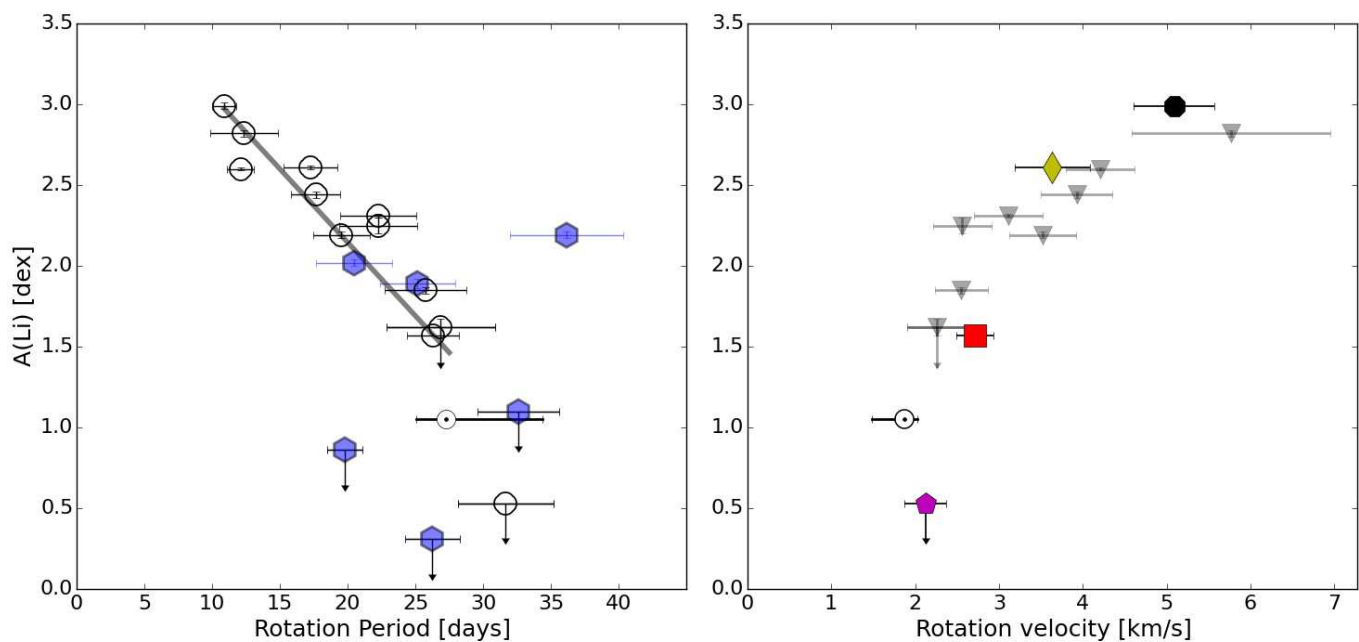


Fig. 5. Lithium abundance versus rotation for the 18 seismic solar analogues. The left and the right panel compare $A(\text{Li})$ with the surface rotation period from space photometry and the computed surface rotation velocity, respectively. Stars found to be located in binaries are shown as filled blue octagons in the left-hand panel and they are removed from the right panel. In both panels, the full range covered by the differential solar rotation is represented by the horizontal error bar in the solar symbol. The solid line in the left panel depicts the best fitting relation for single stars between the rotation period and $A(\text{Li})$ for stars with rotation periods shorter than the solar value. In the right panel, the source of the asteroseismic radius is illustrated through the choice of symbols. Triangle markers indicate stars for which the radius has been determined through global-parameter modelling. Upper limits of the measured $A(\text{Li})$ are shown for stars with low lithium abundance or insufficient S/N in the spectra. The single stars with the radius from detailed modelling from AMP, KIC 10644253, KIC 6116048, KIC 7680114, and KIC 3656476 are plotted as black octagon, yellow diamond, red square and magenta pentagon, respectively.

2.3. Lithium abundance

The $A(\text{Li})$ was derived from the Li I resonance doublet feature at 670.78 nm as depicted for all stars in our sample in Figure 2. We used the ‘synth’ driver of the 2014 version code MOOG (Snedden 1973) and adopted $A(\text{Li})_{\odot} = 1.05$ dex as the standard solar lithium abundance (Asplund et al. 2009). The atmosphere model used were interpolated from the new Kurucz’s grid (Castelli & Kurucz 2004) for a set of spectroscopic atmospheric parameters, T_{eff} , $\log g$, $[\text{Fe}/\text{H}]$, and micro turbulence given in Table 3. We used the Fe I and Fe II absorption lines as specified in Meléndez et al. (2014a), and we neglected possible ${}^6\text{Li}$ influences. Due to the vicinity of the Li lines to the Fe I line at 670.78 nm (blue dotted line in Figure 2), strong Li or iron lines as well as fast rotation can lead to blended lines. Therefore, an accurate value of the iron abundance, the $\log g$, and the projected surface velocity is needed to correctly derive the lithium abundance. The main sources for the Li abundance error are related to the uncertainties on the stellar parameters and the EW measurement. However T_{eff} is by far the dominant source of error. For the spectroscopic atmospheric parameters², we determined the lithium abundance in our sample ranging between 0.06 and 3.03 dex. For comparison, the solar lithium abundance was also derived from the HERMES solar spectrum (Figure 2) collected from the reflected light of the Jovian moon Europa. We measured $A(\text{Li})_{\odot} = 1.06 \pm 0.1$ dex in agreement with Asplund et al. (2009). The final values of $A(\text{Li})$ are listed in the last column of Table 3 and Figure 2. Figure 2 also illustrates the sequence of spectral

² In this work, we use the standard definitions: $[X/Y] = \log(N_X/N_Y) - \log(N_X/N_Y)_{\odot}$, and $A_X = \log(N_X/N_H) + 12$, where N_X is the number density of element X in the stellar photosphere.

segments, containing the two lithium as well as two iron lines for all stars in our sample, sorted by decreasing value of $A(\text{Li})$. For comparison, the solar spectrum obtained by Beck et al. (2016) was plotted at the bottom of the sequence. The comparison between our derived abundances with the values from Bruntt et al. (2012) is presented in Figure 4. A good agreement was found between the values for $A(\text{Li})$. The differences are probably originating from the NLTE effects in the hotter stars (Lind et al. 2009).

2.4. Binarity occurrence

The time span covered by our measurements, as well as the mean value and the dispersion of the radial velocities, are reported in Table 3 for each star in the sample. The measurements range between 260 and 700 days. Based on an earlier analysis of KIC 3241581, Beck et al. (2016) confirmed this star to be a binary with an orbital period longer than 1.5 years. Based on the first 35 days of the observations of this campaign, Salabert et al. (2016a) reported KIC 4914923, KIC 7296438 and KIC 9098294 as binary candidates. Additional spectra were needed to confirm the binarity status of those systems. From the full available dataset analysed in this paper, we confirm the three above mentioned systems are binaries and we report that KIC 10130724 and KIC 7700968 are also binary systems.

For none of the systems a binary period is known yet, because we do not detect the signature of stellar binarity (eclipses or tidally induced flux modulation) in their light curves. Also the RV measurements are too sparsely sampled to derive an orbital period from it. Therefore no meaningful upper or even lower

limit can be proposed on the orbital periods. The mean value reported in Table 2 will roughly resemble the systemic velocity of the binary system. Without information on the orbital parameters, the interpretation of $A(\text{Li})$ in the stellar components of the system is not reliable. Therefore, continuous RV monitoring is required to draw further constraints on the orbital parameters, such as period or eccentricity.

3. Lithium abundance and surface rotation

There is a large number of observational works studying the connection between Li and rotation, searching for correlations between these parameters (e.g. Skumanich 1972; Rebolo & Beckman 1988; King et al. 2000; Clarke et al. 2004; Bouvier 2008; Bouvier et al. 2016). Because of the difficulty in coverage and stability of photometric follow-up observations, most of them have employed $v \sin i$ measurements. Due to the undetermined inclination angle i , such values yield a lower limit on the rotational velocity. The rotation period from the light-curve modulation, such as determined by Krishnamurthi et al. (1998) for the Pleiades or from the modulation of the emission in the core of the Ca H&K lines (e.g. Choi et al. 1995), is independent of the inclination. This, linked to the observational difficulty resolving the tiny absorption line of lithium at 670.7 nm with high S/N for the solar-analogue stars, partially explains the difficulty to connect the dependence between true rotation (rotational period) and the lithium abundance in low-mass, solar-analogues stars at different ages.

In the left panel of Figure 5, the lithium abundance is plotted as a function of the surface rotation period derived from the *Kepler* light curves (García et al. 2014) and surface rotation velocity. For comparison, the Sun is presented by the longitudinal average rotation period of 27 days. The full range of solar differential rotation, spreads between 25 days at the equator and 34 days at the poles (e.g. Thompson et al. 1996), is represented by the horizontal error bar in the solar symbol in Figure 5. From this figure we can see that fast rotating stars have high Li abundances. This confirms the well known general trend for lithium and rotation found in the earlier mentioned studies of clusters and for single field stars (e.g. Skumanich 1972; Rebolo & Beckman 1988; King et al. 2000; Clarke et al. 2004; Bouvier 2008; Bouvier et al. 2016). There is a large scattering for rotation periods longer than the solar rotation period. This is also found in similar studies of clusters and large sample of field stars. In this context, our sample is unique in the sense that for field stars we combine the existing information about the true rotation period, lithium abundance, seismic age and masses, and binarity status. In addition, stellar binarity can affect the measured lithium abundance either through interactions of the components (e.g. Zahn 1994) or due to observational biases. Given that an orbital solution is needed for a complete analysis of such system, we will concentrate on the single stars in this work. This approach reduces the scatter in the $A(\text{Li})$ - P_{rot} plane, if only single stars are taken into account. In the rest of the analysis we only use single stars and stars with P_{rot} below 27 days. For this subsample, the Li-rotation correlation shows a trend following a linear regression,

$$A(\text{Li}) = -(0.08 \pm 0.01) \times P_{\text{rot}} + (3.85 \pm 0.17). \quad (1)$$

This relation indicates that lithium appears to evolve similarly to the rotation velocity for stars on this range of mass and metallicities for $P_{\text{rot}} \lesssim 27$ days. We note that by fitting a trend in the P_{rot} -Li plane, we do not take explicitly into account the age of

the stars. But implicitly, it is taken into account as surface rotation is a proxy of age (Barnes 2007). Although van Saders et al. (2016) showed that stars, once they reach approximately the age of the Sun, are not slowing down as much as predicted by the empirical relations between rotation and stellar age (e.g. Barnes 2007; Gallet & Bouvier 2013, 2015). However gyrochronology is still valid for stars younger than the Sun. Thus, a rotation rate higher than the solar value implies a star younger than the Sun. This is in agreement with the modelled evolution of Li, because the strongest depletion of the lithium surface abundance on the main sequence is taking place in the early stages (e.g. Castro et al. 2016, and references therein; see also Section 5 in this paper).

The evolution of the lithium abundance with the rotation period, as described by Equation (1) is the best fit of the trend for stars with masses $1.0 \lesssim M/M_{\odot} \lesssim 1.1$ and $[\text{Fe}/\text{H}]$ in the range 0.1 to 0.3 dex, (with the exceptions of KIC 10971974 and KIC 6116048, Table 3). The trend is well defined for rotation periods shorter than 27 days. The bulk of stars in our sample is rotating with shorter rotation periods than the Sun. This could be due to a selection bias in which longer periods are more difficult to detect. Besides that, more data seems to be necessary to extrapolate this results for slow rotators (long period) regimes.

Although, two stars with the same angular velocity (as used in the left panel of Figure 5), the rotational velocity still can be different, since it depends on the unknown stellar radius. We can overcome this degeneracy by using the asteroseismic radius (Table 1) to convert the rotation period into the unprojected rotational velocity v_{rot} in kilometers-per-second. In the right panel of Figure 5, we plot the rotational velocity computed as a function of lithium abundance. Because spots can be found at a relatively wide range of latitudes, surface differential rotation might contribute to the scatter in the rotation-lithium relation. Furthermore, the flux modulation introduced by spots, in combination with an assumed solar or anti-solar differential rotation profile will lead to an under or over estimation of the rotational velocity at the equator, respectively (Brun et al. 2015, Brun et al., *subm.*). From the right panel of Figure 5 we find that for stars with rotational velocities higher than 3 km/s a linear trend is found in the Li-velocity relation. Between values of v_{rot} of 2 and 3 km/s, a large dispersion in the measured values of lithium could be present ($A(\text{Li}) \lesssim 2$ dex), engulfing also the position of the Sun in this diagram. Comparing the right panel of Figure 5 to large-sample studies of $v \sin i$, such as Takeda et al. (2010) shows a good agreement. In the asteroseismic approach, the complications introduced by the unknown inclination of the rotation axis or the assumptions on the turbulent velocity fields that could influence the line profile, are eliminated. Applying this asteroseismic approach on large samples should thus reduce the systematic scatter.

4. Discussion

Both observables, rotation and $A(\text{Li})$ are expected to evolve with time for stars of this mass range during the main sequence. This was suggested by Skumanich (1972) from the observations of stars in the Hyades, Pleiades, Ursa Major and the Sun, which were further investigated (e.g. Rebolo & Beckman 1988; King et al. 2000; Clarke et al. 2004). In general, the Li abundance is a function of the convective envelope deepening relative to the age of a star on the main sequence (do Nascimento et al. 2009; Baumann et al. 2010). It can also be the consequence of mixing below the convective zone (Brun et al. 1999) or in the radiative core (Talon & Charbonnel 2005; Charbonnel & Talon

2005). This confirms that the age, the angular momentum history, the mass and the metallicity are the governing physical processes in the evolution of the lithium content. Recently, [Castro et al. \(2016\)](#) showed that in the cluster M67, there is a relatively large scatter of the lithium abundance in the main-sequence stars with the same effective temperature and same age. The scatter is the largest around the $1 M_{\odot}$ -range ($0.5 \lesssim A(\text{Li}) \lesssim 2.0$ dex) and suggests that another, yet unknown process could have an influence on the lithium abundance. [Somers & Pinsonneault \(2016\)](#) suggest that an intrinsically different mixing history than in other stellar clusters, such as a higher fraction of fast rotators or inhomogeneities of the initial rotation distribution ([Coker et al. 2016](#)), could explain the scatter in lithium depletion for stars older than 100 Myr.

4.1. Stellar ages

In a cluster all stars have the same age. This cannot be assumed for the field stars in our sample. As described in Section 2, there are two ways to use the seismic information to infer the age. When grid-modelling based on global-seismic parameters is used, the inferred ages have large uncertainties ([Lebreton & Goupil 2014](#)). In our sample, several of these stars are rotating faster than the Sun ([García et al. 2014](#)), indicating that they should be younger ([Barnes 2007](#); [van Saders et al. 2016](#)). However, some ages are derived from global-parameter seismology, and are larger than the solar age. To avoid these inconsistency problems, in the following analysis, we will only use ages inferred from detailed modelling, constrained by individual frequencies or frequency ratios. As described in Section 2 and listed in Table 1. We have age and mass estimates through this approach for eight stars from studies of [Mathur et al. \(2012\)](#), [Metcalf et al. \(2014\)](#), [Creevey et al. \(2016\)](#) and [García et al. \(in prep.\)](#).

4.2. Comparison with stellar models

To compare the derived stellar age and measured lithium abundance with stellar modelling predictions, a grid of models of the temporal evolution of $A(\text{Li})$ due to rotation-induced mixing using the *Toulouse-Geneva stellar evolution code* (TGEC, [Hui-Bon-Hoa 2008](#); [do Nascimento et al. 2009](#)) was computed.

A description of the physics used for this grid is given in Appendix A. For details on the calculation of the theoretical Li abundance we refer to [Castro et al. \(2009, 2016\)](#), and [do Nascimento et al. \(2009\)](#). These models include the impact of the rotation-induced mixing on chemicals due to the combined actions of meridional circulation and shear-induced turbulence in stellar radiation zones computed as prescribed by [Zahn \(1992\)](#), [Maeder & Zahn \(1998\)](#), [Théado & Vauclair \(2003\)](#) and [Hui-Bon-Hoa \(2008\)](#). This non-standard mixing, modelled as a vertical effective turbulent diffusion applied on chemical elements ([Chaboyer & Zahn 1992](#), and Appendix A), is calibrated to reproduce the solar lithium abundance at the solar age in a solar model (we refer the reader to [Castro et al. 2016](#), for a detailed description of the calibration). The calibration is then used for the other models with different masses and metallicities. In this framework, it is important to point that we focus here only on the non-standard mixing for chemicals (we refer the reader to Appendix A for more details). This rotational mixing and the resulting Lithium abundance strongly depend on internal transport mechanisms (e.g. [Maeder 2009](#); [Mathis 2013](#)) and on angular momentum extraction by stellar winds ([Skumanich 1972](#);

[Matt et al. 2015](#)) as illustrated for example by the recent work by [Amard et al. \(2016\)](#). These processes are here calibrated as explained in Appendix A on the Sun and its rotational history through the effective vertical turbulent diffusion acting on chemicals. This may introduce a bias towards solar characteristics. However this work constitutes a first step. In a near future, more realistic models will be computed where rotational and chemical evolutions will be treated coherently and simultaneously. These models will take into account all angular momentum processes and potentially different rotational histories.

The setup of the input physics used in our models is compatible with the one used in the AMP models. Our models are calculated from the zero-age main sequence (ZAMS) to the helium burning in the core and for masses from 1.0 to $1.15 M_{\odot}$ with a step size of $0.05 M_{\odot}$. The main grid was calculated with a metallicity of $[\text{Fe}/\text{H}] = +0.20$. An additional model of the Li-evolution was calculated for a $1.0 M_{\odot}$ star with $[\text{Fe}/\text{H}] = -0.20$. For comparison, the evolutionary track of the solar model computed by [do Nascimento et al. \(2009\)](#) is shown in Figure 6.

We note that the grid of models contains only representative models chosen for average mass and metallicity. The step size of $0.05 M_{\odot}$ is roughly the averaged uncertainty (7%) of the detailed modelling approach found by [Lebreton & Goupil \(2014\)](#), accounting for the observational uncertainties and those of the model approaches. The authors found also a typical uncertainty of the seismic age estimate of $\sim 10\%$. Therefore, this comparison provides a qualitative idea if the models and the measurements agree in general, but these model tracks are not calibrated to resemble specific stars on a case-to-case basis.

By focusing on stars for which detailed modelling has been performed and were found to be without a companion, our sample is narrowed down to 4 stars, they are – KIC 3656476 (age=8.9 Gyr, $[\text{Fe}/\text{H}] = +0.25$ dex), KIC 6116048 (6.1 Gyr, -0.18 dex), KIC 7680114 (6.9 Gyr, $+0.15$ dex), and KIC 10644253 (0.9 Gyr, $+0.1$ dex). The measured lithium abundances are compared against the stellar age from AMP-modelling for these 4 stars in Figure 6. Here, these three stars KIC 10644253, KIC 7680114 and KIC 3656476, are of particular interest, as they form a sequence of constant mass of $1.1 M_{\odot}$ (within their uncertainties) and a metallicity above the solar value, which spans over stellar ages between 1 and 9 Gyr. With its $1.05 \pm 0.03 M_{\odot}$, KIC 6116048 is closer to the solar mass, but has a clear sub-solar metallicity. In Figure 6 the observed $A(\text{Li})$ is plotted as a function of the estimated age from asteroseismology and compared to the predictions of these quantities from the above described model tracks.

4.2.1. Case of KIC 10644253

The comparison depicted in Figure 6 shows that the best agreement between measurements and models for age and lithium is found for KIC 10644253. The measured activity levels as well as the short rotation period reported by [Salabert et al. \(2016a,b\)](#) further confirm that this is a young stellar object.

4.2.2. Case of KIC 7680114

KIC 7680114 complies reasonably well with the evolutionary track of a star of $1.1 M_{\odot}$ with a metallicity of $+0.2$ dex. The star has a rotation period of 26.3 days, compatible with the solar one. The asteroseismic modelling places it at ~ 7 Gyr, about 2.5 Gyr older than the Sun. [van Saders et al. \(2016\)](#) show that when increasing mass or temperature the reduced efficiency of magnetic breaking starts earlier, which may explain this discrepancy.

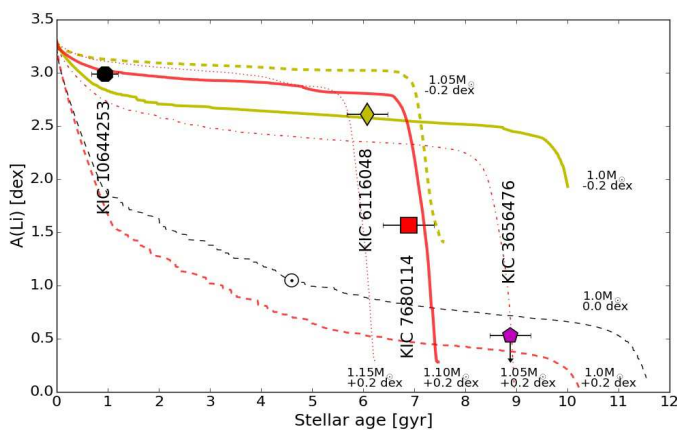


Fig. 6. Lithium abundance of single stars with age computed by detailed modelling with the AMP code. The stars KIC 10644253, KIC 6116048, KIC 7680114, and KIC 3656476 are plotted as black hexagon, yellow diamond, red square and magenta pentagon, respectively. For KIC 3656476 the upper limits of the measured $A(\text{Li})$ is shown. TGEC-evolutionary tracks shown in red, and yellow represents the theoretical evolution of $A(\text{Li})$ for models of the indicated mass with $[\text{Fe}/\text{H}] = +0.2$, and -0.2 dex, respectively. The black dashed evolutionary track depicts the evolution of Li calculated by do Nascimento et al. (2009) and the solar marker depicts measured $A(\text{Li}_\odot)$ and age of the Sun.

4.2.3. Case of KIC 3656476

The slowly rotating star KIC 3656476, is confirmed from stellar modelling and the comparison with the lithium abundance to be an old object. Although the $1.1 M_\odot$ evolutionary track of the TGEC modelling does not reach the age predicted by the AMP model it is not a worrying disagreement. Taking the typical uncertainty of $\sim 7\%$ on the seismic mass estimate, we find a good agreement with the Li evolution for a $1.05 M_\odot$ star. Such uncertainty corresponds to 2σ of the mass uncertainty of the star's model reported by Creevey et al. (2016).

4.2.4. Case of KIC 6116048

For KIC 6116048, the rotation period of ~ 10 days shorter than the value of the Sun suggests that this is a young star (García et al. 2014). On the other hand, this star is one of the lowest active stars in our sample (Salabert et al. 2016a) and the seismic modelling suggests an age of 6 Gyr (Creevey et al. 2016). In principle, it is possible that the rotation period from the literature could be half of the actual value (García et al. 2014). In such case however, this star would fall out of the observed relation between P_{rot} and $A(\text{Li})$.

Despite the non-agreement of the age indicators, we find a general good agreement between $A(\text{Li})$ measurement and the models. Within the conservative view on the uncertainty of the mass, the measured $A(\text{Li})$ is in good agreement with the theoretical Li evolution for a 1.0 and $1.05 M_\odot$ star. Because $A(\text{Li})$ remains relatively constant over a large range in time, Li cannot be used to distinguish between the two scenarios. KIC 6116048 is a puzzling case which definitely needs further investigation.

4.3. Results

From the comparison of the observations with models, calculated for the determined seismic mass, we find $A(\text{Li})$ in good agreement for all four single stars with available AMP modelling.

For the Sun it has been shown that gravity waves have to be included in order to reproduce the solar rotation and lithium profile (Charbonnel & Talon 2005). Although gravity waves were not explicitly included in the applied macroscopic hydrodynamical mixing modelling, they were implicitly taken into account through the calibration of the models to the Sun. The good agreement of measured and modelled $A(\text{Li})$ in Figure 6 shows that the four stars share the same internal physics as it is working in the Sun.

5. Conclusions

In this work, we have presented the combined analysis of seismic, photometric, and spectroscopic values for a set of 18 solar-analogue stars. The sample is important and unique, as not only for the lithium abundance and the rotation period are known, but also for the mass, radius and age estimates for all stars from seismology. The rotation periods and seismic parameters used in this study were determined by several earlier studies (Mathur et al. 2012; García et al. 2014; Chaplin et al. 2014; Metcalfe et al. 2014; Creevey et al. 2016, Garcia et al. in prep.). For an overview of the literature values and references please see Table 1. In a dedicated observing campaign we obtained high-resolution spectroscopy with the HERMES échelle spectrograph, allowing us to determine a consistent set of spectroscopic fundamental parameters, including the Li surface abundance. From our spectroscopic observations, we detected six new binary systems.

The surface abundance of lithium of a star is very sensitive to its rotation rate, mass, and metallicity. Masses from asteroseismology allows us to select our targets accurately on the criterion of mass. Choosing a sample of stars within the very narrow mass range, which is accepted as a solar-analogues, enables us to study the interplay of these parameters. From the sample of single stars, we could quantify a linear relationship between the rotation period and the $A(\text{Li})$ for rotation periods shorter than the solar one. Binary stars show a larger scatter in the parameter plane. We demonstrated that observational restriction can be overcome by calculating the actual rotational velocity v_{rot} using the asteroseismically determined radius of the star. This allows a better comparison with model predictions.

By focusing on 4 single stars with available masses and robust ages from detailed modelling with the AMP-code and confronting them with TGEC evolutionary track for the lithium abundance, we confirm the high degree of sensitivity of $A(\text{Li})$ to the combination of stellar mass, metallicity, rotation rate and age. For two of the 'massive' solar analogues ($\sim 1.1 M_\odot$) with detailed modelling, KIC 10644253 and KIC 7680114, the measured $A(\text{Li})$ and the stellar mass and age from asteroseismology agree well with the predicted Li abundance. For the third 'massive' solar analogue, KIC 3656476, a good agreement is found within the conservative mass uncertainty of $\sim 7\%$. A similar case is the solar-analogue with sub-solar metallicity, KIC 6116048. Also for this star we find a good agreement with the modelled evolution of $A(\text{Li})$ within the conservative mass uncertainty. The measured value of $A(\text{Li})$ agrees with the plateau value found for $1.0 M_\odot$ star but the rotation period indicates a young object while seismology suggest a target, older than the Sun. In principle the rotation period could be underestimated by a factor of two, which however would lead to a strong outlier in the $P_{\text{rot}}-A(\text{Li})$ relation, depicted in Figure 5.

The comparison of $A(\text{Li})$ with age and the rotation rate demonstrates that gyrochronology is valid for stars younger than the Sun and until the age of the Sun. The small number of stars

with individual-frequency modelling does not allow us to draw further conclusions on their evolution with age. A larger dataset will be required to confirm the conclusions outlined here.

For these genuine solar analogues, a good agreement within the uncertainties is found between three independent approaches – the observed A(Li) from spectroscopy, the stellar age and mass from asteroseismology as well as the stellar model prediction of A(Li) for representative TGEC-models. Because the TGEC-models for A(Li) were calibrated to reproduce the solar internal mixing, such consensus with the measured A(Li) in the solar analogues may indicate that the solar analogues share the same acting internal mixing than the Sun. In this light, the solar value of A(Li) is absolutely normal.

Acknowledgements. We thank the referee for his/her constructive report that allows us to improve the article. We acknowledge the work of the team behind *Kepler* and *MERCATOR*. PGB and RAG acknowledge the ANR (Agence Nationale de la Recherche, France) program IDEE (n° ANR-12-BS05-0008) "Interaction Des Etoiles et des Exoplanetes". PGB and RAG also received funding from the CNES grants at CEA. JDN, MC and TD acknowledge the CNPq and the PPGF/UFRN. PGB acknowledges the PPGF/UFRN for founding partially a scientific visit to the G3 team at UFRN, Natal, Brazil. DS and RAG acknowledge the financial support from the CNES GOLF and PLATO grants. DM acknowledges financial support from the Spanish Ministerio de Economía y Competitividad under grant AYA2014-54348- C3-3-R. StM acknowledges support by the ERC through ERC SPIRE grant No. 647383. AT received funding from the European Research Council (ERC) under the European Union's Horizon 2020 research and innovation programme (grant agreement N°670519: MAMSIE). SaM would like to acknowledge support from NASA grants NNX12AE17G and NNX15AF13G and NSF grant AST-1411685. The research leading to these results has received funding from the European Community's Seventh Framework Programme (FP7/2007-2013) under grant agreement No. 312844 (SPACEINN) and under grant agreement No. 269194 (IRSES/ASK). The observations are based on spectroscopy made with the *MERCATOR* Telescope, operated on the island of La Palma by the Flemish Community, at the Spanish Observatorio del Roque de los Muchachos of the Instituto de Astrofísica de Canarias. This research has made use of the SIMBAD database, operated at CDS, Strasbourg, France.

References

- Aerts, C., Christensen-Dalsgaard, J., & Kurtz, D. W. 2010, *Asteroseismology*, Springer Science+Business Media B.V.
- Alexander, D. R. & Ferguson, J. W. 1994, *ApJ*, 437, 879
- Allende Prieto, C., Beers, T. C., Wilhelm, R., et al. 2006, *ApJ*, 636, 804
- Amard, L., Palacios, A., Charbonnel, C., Gallet, F., & Bouvier, J. 2016, *A&A*, 587, A105
- Angulo, C., Arnould, M., Rayet, M., et al. 1999, *Nuclear Physics A*, 656, 3
- Asplund, M., Grevesse, N., Sauval, A. J., & Scott, P. 2009, *ARA&A*, 47, 481
- Barklem, P. S. 2007, *A&A*, 466, 327
- Barklem, P. S. & O'Mara, B. J. 2001, *Journal of Physics B Atomic Molecular Physics*, 34, 4785
- Barnes, S. A. 2007, *ApJ*, 669, 1167
- Basu, S. & Antia, H. M. 1997, *MNRAS*, 287, 189
- Baumann, P., Ramírez, I., Meléndez, J., Asplund, M., & Lind, K. 2010, *A&A*, 519, A87
- Beck, P. G., Allende Prieto, C., Van Reeth, T., et al. 2016, *A&A*, 589, A27
- Bensby, T., Feltzing, S., & Oey, M. S. 2014, *A&A*, 562, A71
- Böhm-Vitense, E. 1958, *ZAp*, 46, 108
- Bouvier, J. 2008, *A&A*, 489, L53
- Bouvier, J., Lanzafame, A. C., Venuti, L., et al. 2016, *A&A*, 590, A78
- Brun, A. S., García, R. A., Houdek, G., Nandy, D., & Pinsonneault, M. 2015, *Space Sci. Rev.*, 196, 303
- Brun, A. S., Turck-Chièze, S., & Zahn, J. P. 1998, in *Structure and Dynamics of the Interior of the Sun and Sun-like Stars SOHO 6/GONG 98 Workshop*, 439–443
- Brun, A. S., Turck-Chièze, S., & Zahn, J. P. 1999, *ApJ*, 525, 1032
- Bruntt, H., Basu, S., Smalley, B., et al. 2012, *MNRAS*, 423, 122
- Carlos, M., Nissen, P. E., & Meléndez, J. 2016, *A&A*, 587, A100
- Castelli, F. & Kurucz, R. L. 2004, *arXiv:astro-ph/0405087*
- Castro, M., Duarte, T., Pace, G., & do Nascimento, Jr., J. D. 2016, *A&A*, 590, A94
- Castro, M., Vauclair, S., Richard, O., & Santos, N. C. 2009, *A&A*, 494, 663
- Cayrel de Strobel, G. 1996, *A&Ar*, 7, 243
- Chaboyer, B. & Zahn, J.-P. 1992, *A&A*, 253, 173
- Chaplin, W. J., Basu, S., Huber, D., et al. 2014, *ApJS*, 210, 1
- Chaplin, W. J., Kjeldsen, H., Christensen-Dalsgaard, J., et al. 2011, *Science*, 332, 213
- Chapman, S. 1917, *MNRAS*, 77, 540
- Charbonnel, C. & do Nascimento, Jr., J. D. 1998, *A&A*, 336, 915
- Charbonnel, C. & Talon, S. 2005, *Science*, 309, 2189
- Charbonnel, C., Vauclair, S., Maeder, A., Meynet, G., & Schaller, G. 1994, *A&A*, 283, 155
- Choi, H.-J., Soon, W., Donahue, R. A., Baliunas, S. L., & Henry, G. W. 1995, *PASP*, 107, 744
- Clarke, D., MacDonald, E. C., & Owens, S. 2004, *A&A*, 415, 677
- Coker, C. T., Pinsonneault, M., & Terndrup, D. M. 2016, *ApJ*, 833, 122
- Creevey, O., Metcalfe, T. S., Schultheis, M., et al. 2016, *ArXiv*: 1612.08990
- Datson, J., Flynn, C., & Portinari, L. 2014, *MNRAS*, 439, 1028
- Delgado Mena, E., Israelian, G., González Hernández, J. I., et al. 2014, *A&A*, 562, A92
- do Nascimento, Jr., J. D., Castro, M., Meléndez, J., et al. 2009, *A&A*, 501, 687
- do Nascimento, Jr., J. D., da Costa, J. S., & de Medeiros, J. R. 2010, *A&A*, 519, A101
- dos Santos, L. A., Meléndez, J., do Nascimento, J.-D., et al. 2016, *A&A*, 592, A156
- Eddington, A. S. 1916, *MNRAS*, 77, 16
- Eddington, A. S. 1926, *The Internal Constitution of the Stars*
- Ekström, S., Georgy, C., Eggenberger, P., et al. 2012, *A&A*, 537, A146
- Epstein, C. R., Johnson, J. A., Dong, S., et al. 2010, *ApJ*, 709, 447
- Fuhrmann, K., Axer, M., & Gehren, T. 1993, *A&A*, 271, 451
- Gallet, F. & Bouvier, J. 2013, *A&A*, 556, A36
- Gallet, F. & Bouvier, J. 2015, *A&A*, 577, A98
- García, R. A., Ceillier, T., Salabert, D., et al. 2014, *A&A*, 572, A34
- GarcíaLopez, R. J. & Spruit, H. C. 1991, *ApJ*, 377, 268
- Gehren, T. 1981, *A&A*, 100, 97
- Grevesse, N. & Noels, A. 1993, in *Perfectionnement de l'Association Vaudoise des Chercheurs en Physique*, ed. B. Hauck, S. Paltani, & D. Raboud, 205–257
- Gustafsson, B. 1998, *Space Sci. Rev.*, 85, 419
- Gustafsson, B. 2008, *Physica Scripta Volume T*, 130, 014036
- Hui-Bon-Hoa, A. 2008, *Ap&SS*, 316, 55
- Iglesias, C. A. & Rogers, F. J. 1996, *ApJ*, 464, 943
- King, J. R., Krishnamurthi, A., & Pinsonneault, M. H. 2000, *AJ*, 119, 859
- Krishnamurthi, A., Terndrup, D. M., Pinsonneault, M. H., et al. 1998, *ApJ*, 493, 914
- Lambert, D. L. & Reddy, B. E. 2004, *MNRAS*, 349, 757
- Lebreton, Y. & Goupil, M. J. 2014, *A&A*, 569, A21
- Lehmann, H., Tkachenko, A., Semaan, T., et al. 2011, *A&A*, 526, A124
- Lind, K., Asplund, M., & Barklem, P. S. 2009, *A&A*, 503, 541
- Ludwig, H.-G., Behara, N. T., Steffen, M., & Bonifacio, P. 2009, *A&A*, 502, L1
- Maeder, A. 2009, *Physics, Formation and Evolution of Rotating Stars*
- Maeder, A. & Zahn, J.-P. 1998, *A&A*, 334, 1000
- Mathis, S. 2013, in *Lecture Notes in Physics*, Berlin Springer Verlag, Vol. 865, Lecture Notes in Physics, Berlin Springer Verlag, ed. M. Goupil, K. Belkacem, C. Neiner, F. Lignières, & J. J. Green, 23
- Mathis, S., Palacios, A., & Zahn, J.-P. 2004, *A&A*, 425, 243
- Mathur, S., Metcalfe, T. S., Woitaszek, M., et al. 2012, *ApJ*, 749, 152
- Matt, S. P., Brun, A. S., Baraffe, I., Bouvier, J., & Chabrier, G. 2015, *ApJ*, 799, L23
- Meléndez, J., Bergemann, M., Cohen, J. G., et al. 2012, *A&A*, 543, A29
- Meléndez, J., Ramírez, I., Casagrande, L., et al. 2010, *Ap&SS*, 328, 193
- Meléndez, J., Ramírez, I., Karakas, A. I., et al. 2014a, 791, 14
- Meléndez, J., Schirbel, L., Monroe, T. R., et al. 2014b, *A&A*, 567, L3
- Metcalfe, T. S., Creevey, O. L., & Christensen-Dalsgaard, J. 2009, *ApJ*, 699, 373
- Metcalfe, T. S., Creevey, O. L., Doğan, G., et al. 2014, *ApJs*, 214, 27
- Monroe, T. R., Meléndez, J., Ramírez, I., et al. 2013, *ApJ*, 774, L32
- Pace, G., Castro, M., Meléndez, J., Théado, S., & do Nascimento, Jr., J.-D. 2012, *A&A*, 541, A150
- Paquette, C., Pelletier, C., Fontaine, G., & Michaud, G. 1986, *ApJS*, 61, 177
- Paxton, B., Cantiello, M., Arras, P., et al. 2013, *ApJS*, 208, 4
- Pinsonneault, M. H. 2010, in *IAU Symposium*, Vol. 268, IAU Symposium, ed. C. Charbonnel, M. Tosi, F. Primas, & C. Chiappini, 375–380
- Ramírez, I., Meléndez, J., Bean, J., et al. 2014, *A&A*, 572, A48
- Raskin, G. 2011, PhD thesis, Institute of Astronomy, Katholieke Universiteit Leuven, Belgium
- Raskin, G., van Winckel, H., Hensberge, H., et al. 2011, *A&A*, 526, A69
- Rebolo, R. & Beckman, J. E. 1988, *A&A*, 201, 267
- Reddy, B. E., Tomkin, J., Lambert, D. L., & Allende Prieto, C. 2003, *MNRAS*, 340, 304
- Rieutord, M. 2006, *A&A*, 451, 1025
- Robles, J. A., Lineweaver, C. H., Grether, D., et al. 2008, *ApJ*, 684, 691
- Rogers, F. J. & Nayfonov, A. 2002, *ApJ*, 576, 1064

- Salabert, D., García, R. A., Beck, P. G., et al. 2016a, *A&A*, 596, A31
 Salabert, D., Régulo, C., García, R. A., et al. 2016b, *A&A*, 589, A118
 Schatzman, E. 1996, *Journal of Fluid Mechanics*, 322, 355
 Shulyak, D., Tsymbal, V., Ryabchikova, T., Stütz, C., & Weiss, W. W. 2004, *A&A*, 428, 993
 Skumanich, A. 1972, *ApJ*, 171, 565
 Sneden, C. A. 1973, PhD thesis, The University of Texas at Austin.
 Somers, G. & Pinsonneault, M. H. 2016, *ApJ*, 829, 32
 Sousa, S. G., Santos, N. C., Israelian, G., Mayor, M., & Monteiro, M. J. P. F. G. 2007, *A&A*, 469, 783
 Spiegel, E. A. & Zahn, J. P. 1992, *A&A*, 265, 106
 Sweet, P. A. 1950, *MNRAS*, 110, 548
 Takeda, Y., Honda, S., Kawanomoto, S., Ando, H., & Sakurai, T. 2010, *A&A*, 515, A93
 Talon, S. & Charbonnel, C. 1998, *A&A*, 335, 959
 Talon, S. & Charbonnel, C. 2005, *A&A*, 440, 981
 Théado, S. & Vauclair, S. 2003, *ApJ*, 587, 777
 Thompson, M. J., Toomre, J., Anderson, E. R., et al. 1996, *Science*, 272, 1300
 Tkachenko, A. 2015, *A&A*, 581, A129
 Tkachenko, A., Lehmann, H., Smalley, B., Debusscher, J., & Aerts, C. 2012, *MNRAS*, 422, 2960
 Tsymbal, V. 1996, in *Astronomical Society of the Pacific Conference Series*, Vol. 108, M.A.S.S., Model Atmospheres and Spectrum Synthesis, ed. S. J. Adelman, F. Kupka, & W. W. Weiss, 198
 van den Heuvel, E. P. J. & Conti, P. S. 1971, *Science*, 171, 895
 van Saders, J. L., Ceillier, T., Metcalfe, T. S., et al. 2016, *Nature*, 529, 181
 Zahn, J.-P. 1992, *A&A*, 265, 115
 Zahn, J.-P. 1994, *A&A*, 288, 829

Appendix A: Physics of the TGEC-grid

A grid of models was calculated with the *Toulouse-Geneva stellar evolution code* (TGEC, [Hui-Bon-Hoa 2008](#); [do Nascimento et al. 2009](#)). The initial chemical mixture relative to the hydrogen content was chosen as the solar one from [Grevesse & Noels \(1993\)](#). The equations of state are derived from the OPAL tables ([Rogers & Nayfonov 2002](#)) and we used the OPAL96 opacities tables ([Iglesias & Rogers 1996](#)) completed by the [Alexander & Ferguson \(1994\)](#) low temperature opacities. For the nuclear reaction rates, we used the NACRE compilation ([Angulo et al. 1999](#)) with the Bahcall screening routine.

Convection was modelled according to the [Böhm-Vitense \(1958\)](#) formalism of the mixing-length theory. The mixing-length parameter $\alpha = l/H_p = 1.69$, where l is the characteristic mixing length and H_p is the pressure scale height, is a free parameter which calibrates the radius of a solar model. Below the convective zone, we introduce a convective undershooting with a depth of $0.09 H_p$ so that, in a solar model, the combined mixing reaches the depth deduced by helioseismology ($r_{cz}/R_\odot = 0.713 \pm 0.001$; [Basu & Antia 1997](#)). In the radiative zone, microscopic diffusion, which is the process of element segregation by gravitational and thermal diffusion ([Eddington 1916](#); [Chapman 1917](#)), is treated by using the [Paquette et al. \(1986\)](#) method for collisions between charged ions with a screened coulomb potential. For a complete description of the microphysics used by these models, we refer the reader to [Théado & Vauclair \(2003\)](#); [do Nascimento et al. \(2009\)](#); [Castro et al. \(2016\)](#).

The meridional circulation in stellar radiation zones (e.g. [Eddington 1926](#); [Sweet 1950](#)), which is driven by the internal stresses induced by rotation (e.g. [Zahn 1992](#); [Rieutord 2006](#); [Mathis 2013](#)), is modelled as prescribed by [Zahn \(1992\)](#). [Zahn \(1992\)](#) demonstrated that these meridional flows transport angular momentum, creating shears that become unstable with a stronger turbulent transport in the horizontal direction than in the vertical one because of the stable stratification. As demonstrated by [Chaboyer & Zahn \(1992\)](#), the vertical advection of chemicals by the meridional circulation is transformed into an effective vertical diffusion because of the strong horizontal turbulence. Similarly, the transition layer at the bottom of the convection zone

between its latitudinal differential rotation and the solid-body rotation of the radiative core (the so-called tachocline) undergoes the same strong anisotropic turbulence (with a much stronger turbulent transport in the horizontal than in the vertical direction). The resulting turbulent transport reduces the differential rotation and inhibits its spread deep inside the radiative interior ([Spiegel & Zahn 1992](#)). [Brun et al. \(1998\)](#) showed that the vertical turbulent transport of chemicals in these layers can be modeled by an exponential diffusion coefficient, which is added to the previously described effective vertical turbulent diffusion. The resulting total vertical turbulent diffusion coefficient in the transport equation for the mean concentration of the different chemical species is here calibrated to reproduce the solar lithium abundance in a solar model as in [Castro et al. \(2016\)](#). In our models, we solve only the transport equation for chemicals. The angular momentum history is not computed explicitly since the equation for the transport of angular momentum is not solved in our models, but it is implicitly taken into account through calibration constants of the effective vertical diffusion, which are implicit function of rotation and shear ([Chaboyer & Zahn 1992](#); [Zahn 1992](#); [Hui-Bon-Hoa 2008](#); [Castro et al. 2016](#)).